HAL
archives-ouvertes.fr

Use of ram extruder as a combined rheo-tribometer to study the behaviour of high yield stress fluids at low strain rate

Arnaud Perrot, Yannick Mélinge, Damien Rangeard, Francesca Micaelli, Patrice Estellé, Christophe Lanos

▶ To cite this version:

HAL Id: hal-00716752
https://hal.archives-ouvertes.fr/hal-00716752

Submitted on 17 Sep 2012

1 **USE OF RAM EXTRUDER AS A COMBINED RHEO-TRIBOMETER TO STUDY**

2 **THE BEHAVIOUR OF HIGH YIELD STRESS FLUIDS AT LOW STRAIN RATE**

3

4 A. Perrot[1*], Y. Mélinge[2], D. Rangeard[2], F. Micaelli[3], P. Estellé[3], C. Lanos[3]

5 (1) Laboratoire d'ingénierie des Matériaux de Bretagne, Université de Bretagne Sud, Université Européenne de

6 Bretagne - Centre de Recherche Christiaan Huygens, BP 92116, 56321 LORIENT Cedex, France

7 (2) LGCGM, INSA Rennes, Université Européenne de Bretagne, 20 avenue des buttes de Coësmes, Rennes,

8 France

9 (3) LGCGM, Université de Rennes 1, Université Européenne de Bretagne, 3 rue du clos courtel, Rennes, France

10

11 [*]: Corresponding author

12 **Arnaud Perrot**

13 **Mail: arnaud.perrot@univ-ubs.fr ; Tel: +33 2 97874577; Fax:+33 2 97874576**

14

15 **Abstract:**

16 We propose in this work to provide an efficient and simple extruder device able to evaluate

17 the rheological and tribological behaviour of high yield stress fluids, such as extrudible

18 materials. An extruder able to measure simultaneously both the friction force acting on the

19 extruder wall and the total extrusion force is developed. Based on previous studies, an

20 efficient and accurate method of data analysis is then proposed and applied in order to obtain

21 both a flow curve and a tribological law. Experimental tests are performed on soft modelling

22 clay, kaolin paste and cement-based materials. Results are compared to conventional

23 rheometry measurements. This comparison helps to evaluate the accuracy of the proposed

24 experimental device and procedure.

25

26 **Keywords:** Extrusion, rheology, tribology, yield stress.

27 **Nomenclature**

28 d: Die orifice diameter (m)

29 D: Extruder barrel diameter (m)

30 F: Total extrusion force recorded at the ram (N)

31 F_{fr}: Friction force on the extruder barrel (N)

32 F_{pl}: Shaping force required to ensure the flow in the die land (N)

33 F_{pl1}: Contribution of F_{pl} induced by the bulk deformation in the shaping zone (N)

34 F_{pl2} : Contribution of F_{pl} induced by the friction acting along the dead zone surface (N)

35 F_{pl3}: Contribution of F_{pl} induced by the friction along the exit orifice surface (N)

36 h_c : Height of the cylinder tool (m)

37 h_v: Height of the vane tool (m)

38 k_{fr}: Apparent friction factor $(Pa.(s.m^{-1})^{nfr})$

39 k_s: Shear consistency -Herschel-Bulkley behaviour $(Pa.s^n)$

40 K_w: Wall friction stress (Pa)

41 K_{w0}: Wall friction yield stress (Pa)

42 L_B: Length of remaining billet (m)

43 L_{dz}: Static or dead zone length (m)

44 L_O: Exit orifice length (m)

45 m: Ratio of the wall friction stress to the bulk shear stress

46 M: Maximum torque recorded during vane tests (N.m)

47 n_{fr}: Friction index

48 n_s: Shear flow index -Herschel-Bulkley behaviour

49 R_c: Radius of the cylinder (m)

50 R_t: Valley to peak value of the surface roughness profile (m)

51 R_v: Radius of the vane tool (m)

52   V: Ram velocity (m.s^{-1})

53   V_i: Velocity at the interface between extruder wall and material billet (m.s^{-1})

54    $\dot{\gamma}$: Shear rate (s^{-1})

55   θ: Conical die entry defined as half the included angle of the dead zone

56   σ_0: Bulk elongational yield stress (Pa)

57   τ: Bulk shear stress (Pa)

58   τ_0: Bulk shear yield stress (Pa)

59

60   **1.   Introduction**

61

62   Extrusion is a highly efficient forming process used in a wide range of industries such as food

63   engineering, ceramics, pharmaceutics, building materials, etc. The extrusion flow properties

64   are directly linked to the material rheology and tribology. An accurate evaluation of the

65   rheological and tribological behaviour of the extruded materials is crucial in order to optimize

66   the process.

67   In Händle's book on ceramics extrusion, ram extrusion is defined as a discontinuous shaping

68   process in which a plastic material is pushed through a die or matrix by a piston, whereby the

69   geometry of the die determines the extrudates profiles (Doll et al. 2007). The use of a ram

70   extruder as a rheometer has already been studied many times (Avitzur 1983; Basterfield et al.

71   2005; Benbow and Bridgwater 1993; Hill 1950; Horrobin 1999; Mimoune and Aouadja 2004;

72   Toplak et al. 2007; Li and Bridgwater 2000; Benbow et al. 1991).

73   In this study, we focus on the development and the use of a ram extruder device dedicated to

74   the study of the rheological and tribological behaviour of high yield stress fluids. The

75   developed apparatus is able to provide independently the wall shear stress at the

76   paste/extruder barrel interface and the pressure required in the die land while common

77 capillary rheometer only provides the total pressure drop required to ensure the flow in the die

78 land. This is of great interest because data analysis of common capillary tests requires

79 assumptions or tests performed with different die geometry in order to separate the pressure

80 drop contribution due to the wall friction from the contribution due to plastic deformation in

81 the shaping area.

82 In a first approach, Benbow and Bridgwater (Benbow and Bridgwater 1993) and Hill (Hill

83 1950) have used the ram extrusion geometry as a tool providing a comparative parameter (for

84 example "extrusion pressure" or "bulk yield stress") which is directly linked to the die

85 pressure drop. These studies have contributed to improve the ideal work equation used for

86 plastic materials. The effect of ram velocity can also be studied with such data analysis

87 methods (Benbow and Bridgwater 1993).

88 Those methods only provide comparative parameters which depend on the ram extruder

89 geometry as shown by recent studies (Basterfield et al. 2005; Toplak et al. 2007). For

90 example, the measured values of extensional yield stress can be far larger than the extensional

91 yield stress of the material computed from rotational rheometry (Srinivasan et al. 1999; Zhou

92 and Li 2005a). However, those methods are the most widely used with a ram extruder and

93 have been used in several studies to analyse the extrudabilty of materials or to evaluate the

94 material's flow behaviour (Alfani and Guerrini 2005; Cheyne et al. 2005; Martin et al. 2006;

95 Mascia et al. 2006; Rahman et al. 2002; Srinivasan et al. 1999; Zhou and Li 2005a; Zhou and

96 Li 2005b).

97 For plastic material and using plastic theory and slip lines analysis, several studies provide

98 more accurate modelling of the force required to overcome the diameter variation using the

99 material elongational yield stress. Those methods require assumptions on the velocity field,

100 slip line design and limit conditions. This was attempted by Horrobin (Horrobin 1999;

101   Horrobin and Nedderman 1998), Avitzur (Avitzur 1983) or Kobayashi and Thomsen

102   (Kobayashi and Thomsen 1963).

103   In recent studies, theoretical frames have been developed to compute intrinsic rheological

104   parameters such as yield stress, consistency or flow index from extrusion tests.

105   For example, Basterfield et al. (Basterfield et al. 2005) proposed an adaptation of the Gibson

106   equations (Gibson 1988) which is used to compute the viscosity and flow index of a power

107   law fluid from orifice extrusion force data. The authors assume a radially convergent flow

108   from the extruder body to the exit die. The proposed model assumed the converging flow to

109   be purely elongational.

110   Toplak et al. (Toplak et al. 2007) have recently developed a new method to compute the yield

111   stress of a material from its gravity draining through an orifice. The authors assume the flow

112   to be similar to the Poiseuille flow through a cylindrical barrel with a diameter equal to the

113   exit die one. The proposed model assumes a shear flow and was successfully applied to wide

114   bore capillary rheometer with small die cross sections.

115   Extrusion is also greatly influenced by the material tribology as shown in several studies

116   (Estellé et al. 2006; Mankar et al. 2004; Perrot et al. 2006; Toutou et al. 2005). Friction may

117   occur in the die land area (Benbow and Bridgwater 1993), but also between the extruder

118   barrel and the material billet as shown in (Mankar et al. 2004; Perrot et al. 2006). Moreover,

119   for high solid volume content materials such as cement-based material, friction forces are the

120   the most important resistant force to overcome in order to ensure the extrusion flow. As a

121   consequence, it is crucial to study what happened far from the die land. This means that the

122   tribological behaviour of the material has to be determined.

123   This leads to the conclusion that the total extrusion force can be split into two contributions:

124   the force required to overcome the diameter decrease and the force required to overcome the

125   friction force acting on the extruder barrel.

126   In this study, we propose to design a novel ram extruder which makes it possible to study both

127   rheological and tribological behaviour of high yield stress fluids (shear yield stress larger than

128   1 kPa). The developed apparatus is able to measure simultaneously the friction force between

129   the extruder and the material billet and the total extrusion force. This extruder is then tested

130   on three different materials: a cement-based material, a kaolin clay paste and commercial soft

131   modelling clay. An adaptation of the model developed by Basterfield et al. is done

132   (Basterfield et al. 2005) to obtain an accurate estimation of the rheological modelling

133   parameters taking into account the friction acting along the dead zone (which acts as a tapered

134   die).

135   **2.   Materials and protocols**

136

137   **2.1. Tested materials**

138   Three pasty materials are tested. They exhibit a yield stress ranging from 15 to 50 kPa. The

139   first one is a commercial soft modelling clay which is known to exhibit a viscoplastic

140   behaviour with negligible elastic properties after short compression (Estellé et al. 2006). The

141   second material is a mix of kaolin clay powder and water (water/kaolin mass ratio equal to

142   38%). The kaolin clay used is a Powdered Polwhite BB from Imerys (Kaolins de Bretagne,

143   Ploemeur, France). The largest clay grain size is close to 40 μm. The mass mean kaolin grain

144   size is close to 9 μm. The third material is a cement-based material containing a large amount

145   of fly ash. The dry powder consists in a mix of 70% of fly ash and 30% of cement. The fly

146   ash has an optimized grain size distribution (mix between micronised and natural) and the

147   cement is an Italcementi type I 52.5 R. The liquid phase is composed by tape water (96 % in

148   mass) and methylcellulose 4% in mass). Such admixture is a polymeric suspension acting as a

149   viscosity enhancer agent in order to reduce drainage. Tests on cement-based paste are

150 performed without delay after mixing in order to avoid rheological changes due to chemical

151 effects.

152 In the present study, the paste compressibility has been neglected. This assumption is

153 supported by two main reasons. Firstly, the study does not concern highly viscous polymer

154 melts which are very sensitive to pressure (Park et al. 2008; Dealy 1995). Secondly, the

155 compressibility effects in the die land remain limited because the recorded pressures are

156 relatively low (under 500 kPa). Such hypothesis seems to be relevant in the present study but

157 it cannot be held in high pressure capillary flow of firm polymer pastes (Mitsoulis and

158 Hatzikiriakos 2009; Mitsoulis et al. 2007).

159 The rheological behaviour of the three tested pastes is visco-plastic. It is important to note that

160 the extruder is efficient only if the tested material remains homogeneous. Thus, it is crucial to

161 check that no drainage occurs during the test. A possible drainage may prohibit the use of the

162 tested device at low ram velocity (Martin et al. 2006; Mascia et al. 2006; Perrot et al. 2007;

163 Perrot et al. 2009; Yu et al. 1999). This can be done by measuring the densities of both the

164 extrudates and the remaining material in the extruder.

165 Reference shear flow measurements have been independently performed under isothermal

166 conditions (20°C) using a Brookfield Soft/Solid tester equipped with a vane geometry in an

167 infinite cup (200x200 mm²). This type of cup is used to circumvent the wall slip artefact. The

168 radius of the four-bladed vane geometry is 4 mm and its height is 8 mm. The shear yield

169 stress is estimated at low shear rate using the stress growth test (Liddel and Boger 1996).

170 Tests are conducted under a rotation rate controlled mode. The tool rotation rate is set at 0.01

171 rad.s^{-1}. This rotation rate is in agreement with the Lidell and Boger protocol and allows for an

172 accurate determination of the yield stress (viscous effects neglected). As proposed by Estelle

173 et al., the end effet is neglected (Estellé et al. 2008). The shear yield stress τ_0 is deduced using

174 equation (1).

175 $$\tau_0 = \frac{M}{2\pi R_v^2 h_v}$$ (1)

176 where M is the maximum recorded torque and R_v and h_v the vane radius and height.

177 Vane measurements provide shear yield stress of 15 ± 1 kPa, 25 ± 2 kPa and 50 ± 4 kPa for

178 the cement based material, the kaolin paste and the soft modelling clay, respectively. Because

179 such materials can exhibit viscous behaviour, a Herschel-Buckley model is used in the

180 following, making it possible to describe possible shear-thinning or shear-thickening

181 behaviour:

182 $$\tau = \tau_0 + k_s \dot{\gamma}^{n_S}$$ (2)

183 where $\dot{\gamma}$, k_s and n_S are respectively the shear rate, the consistency and the flow index.

184 For the tribological behaviour, it has been shown that high yield stress fluids exhibit a friction

185 yield stress value (Roussel and Lanos 2003). The main hypothesis is based on purely plastic

186 flow theory where the friction stress against a steel smooth surface (roughness height, R_t up

187 to3 μm) is considered to be a fraction of the shear stress which strongly depends on the

188 surface roughness (Avitzur 1983; Horrobin 1999). This assumption has been successfully

189 applied to model the squeeze flow of viscoplastic materials (Sherwood and Durban 1996,

190 1998). The friction yield stress, denoted K_{w0}, is measured using the stress growth test

191 procedure used for the shear yield stress measurement (low rotating velocity to avoid velocity

192 influence) replacing the vane tool by a smooth steel cylinder ($R_C = 4$ mm and $h_C = 4$ mm).

193 The friction yield stress is also determined by means of the back extrusion technique. The

194 surface roughness of the back extrusion device and the extruder barrel are equivalent (Perrot

195 et al. 2011). The soft modelling clay exhibits a friction yield stress value of 30 ± 2 kPa with

196 both techniques. For kaolin, the measured friction yield stress value is 9.5 ± 0.5 kPa with the

197 rotating smooth cylinder and 9 ± 1 kPa with the back extrusion technique. This shows that

8

198 both techniques provide equivalent results. The friction yield stress has not been measured for

199 the cement-based mix.

200 Then the velocity effect is highlighted using an analogy with the rheological behaviour. A

201 Herschel-Buckley-like equation has already been used by Benbow and Bridgwater to analyse

202 the friction stress inside a die capillary geometry (Benbow and Bridgwater 1993). The

203 proposed equation can be written as follows:

204 $$K_w = K_{w0} + k_{fr}.V_i^{n_{fr}}$$ (3)

205 Where V_i is the velocity at the interface, k_{fr} is the apparent friction factor and n_{fr} the friction

206 index.

207

208 **2.2. High yield stress materials flowing through ram extruder**

209 In order to develop an efficient extruder to study the material flow behaviour, it is crucial to

210 understand the flow properties of a high yield stress fluids in an axisymetrical ram extruder.

211 The properties of extrusion flow of high yield stress fluids have already been studied through

212 various techniques: MRI (Götz et al. 2003; Rabideau et al. 2010; Barnes et al. 2006), positron

213 emission particle tracking (Wildman et al. 1999), visual observations (Hill 1950; Perrot et al.

214 2007) or numerical simulations (Horrobin 1999; Horrobin and Nedderman 1998; Jay et al.

215 2002; Zienkiewicz et al. 1977). From those studies conducted at low shear rate, axisymetrical

216 extrusion flow can be divided into three parts (Fig. 1):

217 - A plug flow located in the extruder barrel where the paste seems to slip along the wall. This

218 slippage induces friction force that should be overcome to ensure the extrusion flow.

219 - A tapered static zone where the material remains blocked around the die entry. This area is

220 called the "dead zone". It is assumed that the dead zone acts as a conical or tapered entry die

221 as proposed in previous studies (Basterfield et al. 2005; Horrobin 1999).

222   - A forming zone, located inside the conical dead zone, where the material billet diameter

223   decreases. This zone is called the "shaping zone".

224   Thus, it appears obvious to introduce representative force for each part of the flow where

225   material advance and forming occurs (as shown in figure 1):

226   - The shaping force required to give its final shape to the material in the shaping zone,

227   denoted F_{pl} has been the subject of numerous studies (Avitzur 1983; Basterfield et al. 2005;

228   Benbow and Bridgwater 1993; Gibson 1988; Hill 1950; Horrobin 1999; Horrobin and

229   Nedderman 1998; Kobayashi and Thomsen 1963; Benbow et al. 1991) .

230   - The wall friction force F_{fr}, developed along the extruder body F_{fr} is linked to the friction

231   stress value K_w.

232   The reference pressure is the external pressure $P_{atm}=0$. As described in figure 1, L_{dz} denotes

233   the dead zone length and L_B is the friction length. The length of the dead zone is known to

234   depend on both die and extruder body diameters. It is commonly considered that the conical

235   dead zone is characterised by a $\pi/4$ angle. In his study, Basterfield et al. have showed that the

236   variation of this angle between $\pi/3$ and $\pi/6$ has only little effect on the extrusion pressure. As

237   a result, the dead zone length can be modelled as follows (Basterfield et al. 2005; Mascia et

238   al. 2006):

239   $$L_{dz} = \frac{D-d}{2} \qquad (4)$$

240   This assumption is in agreement with the modelling results reported in previous studies

241   (Avitzur 1983; Basterfield et al. 2005; Benbow and Bridgwater 1993; Gibson 1988; Hill

242   1950; Horrobin 1999; Horrobin and Nedderman 1998; Kobayashi and Thomsen 1963).

243   However, L_{dz} is also largely influenced by the roughness of the extruder barrel and die

244   surface. As shown by Horrobin (Horrobin 1999), the roughness of the extruder walls largely

245   influences the dead zone length and form. As a result, it is required to measure the dead zone

246   length after extrusion to check if eq. (4) is valid for a given extruder/material couple.

247   As shown in figure 2, the dead zone length can also be measured from the visualisation of the

248   soft modelling clay remaining in the extruder after extrusion. The dead zone presents little

249   curvature however we assumed that both dead zone length and form are close to the modelled

250   conical one.

251

252   **2.3. Extrusion device and tests**

253   The developed ram extruder shown on figure 3 must be able to measure simultaneously both

254   force contributions: the shaping force acting in the shaping zone and the friction forces acting

255   on the extruder barrel.

256   The extruder barrel consists of a vertical steel barrel of 300 mm in length and 43.3 mm in

257   diameter (denoted D) placed under a controlled velocity load frame. The surface roughness of

258   the barrel is $R_t = 3$ μm and represents the maximum peak to valley height of the roughness

259   profile. A nylon ram is used to push the material inside the barrel, ensures a uniform pressure

260   on the material and avoids liquid drainage upward the ram. This ram is equipped with a 20 kN

261   load cell (with a 1 N accuracy) in order to measure the total extrusion force F required to

262   overcome both frictions on the extruder barrel and shaping force in the die land.

263   The extruder barrel is placed on a novel die system which is fixed on the load frame. This

264   system allows measuring the friction force acting along the barrel wall. The bottom of the

265   extruder barrel and the top of the die system are both equipped with similar circular shoulders

266   of diameter 100 mm. The shoulders are perforated by three holes (diameter 6 mm – 120°

267   oriented) and connected using three small perforated cylindrical 2 kN load cells which are

268   centred on the holes (diameter 20 mm, hole diameter 6 mm, thickness 3 mm, and 1 N

269   accuracy). Those load cells are pre-stressed by a screw-bolt system.

270   During extrusion, the material billet induces a wall friction stress on the extruder barrel which

271   tends to move the barrel downward toward the die and consequently squeezes the three load

272 cells. The sum of the three recorded forces is considered to be equal to the friction force F_{fr}

273 acting on the extruder barrel surface.

274 Then, the shaping force can be deduced from the measured values of both the total extrusion

275 force measured at the ram and the friction force measured by the load cells supporting the

276 barrel.

277 The friction force measurement requires some geometrical adjustments:

278   - The length of the barrel should be greater than its diameter in order to give sufficient

279   surface for the measurement of the friction acting on the barrel surface.

280   - The die diameter should be at least 10 times the maximum particle diameter in case of

281   suspensions extrusion.

282   - According to eq. (4), low extrusion ratio d/D (less than 0.1) leads to high value of L_{dz}.

283   Then the dead zone may enter the friction measurement zone. In this case, use of wide

284   bore capillary rheometer analysis should be preferred (Toplak et al. 2007).

285 This third geometrical limitation is crucial. If the dead zone is long enough to enter the barrel,

286 the force measured by the three small load cells will not exactly correspond to the friction

287 linked to the moving material and then will not provide an accurate value of the wall friction

288 stress. In order to avoid this measurement artefact, a zone of 20 mm in length is placed

289 between the exit orifice (square angle die) and the extruder barrel. With the used die

290 diameters (denoted d) of 8, 15 and 20 mm and using eq. (4) the computed dead zone length

291 ranges from 11.5 to 17.65 mm (which is less than 20 mm). This ensures that the dead zone

292 does not obstruct the movement due to the friction force at the flowing material/barrel

293 interface.

294 The die land is 8 mm long. Wall Friction on the die land surface has to be subtracted from the

295 measured shaping force in order to study the work done in the conical zone where the material

296 diameter is shaped. The procedure will be presented in the shaping force analysis section.

297   A 55.3 mm diameter extrusion barrel with common square angle dies is also used in addition

298   to the 43.3 mm diameter developed extruder. It is done to verify if the proposed data analysis

299   depends on the extruder geometry.

300   Extrusion tests are carried out under a load frame ensuring a constant ram velocity ranging

301   from 0.1 mm.s^{-1} to 8.33 mm.s^{-1}.

302   The material billet length is controlled and ranges from 120 to 200 mm depending on the test.

303   Both extruder barrels can be used with three different square angle exit dies that allow for

304   performing tests at the same extrusion ratios (i.e. d/D equals to 0.18, 0.34 and 0.45). The final

305   volume and mass are measured and the computed apparent density is compared to the

306   theorical density.

307

308   **3.   Experimental results analysis**

309

310   **3.1. Extruder device validation and force data analysis**

311   An illustration of the total extrusion force versus the remaining billet length is presented in

312   figure 4. The curve can be split into three distinct parts. The first part consists in the flow

313   initiation. At the beginning of extrusion, the billet length is at its maximum. When the ram

314   starts to move, the billet is compacted. As a result, the recorded extrusion force dramatically

315   increases. We consider that this step ends when the extrusion force reaches its maximal value.

316   Then the second part begins. The extrusion force starts to linearly decrease as the ram

317   advances (i.e. as the remaining billet length decreases). Such particular force versus billet

318   length evolution can be observed because the fluid is mainly plastic and remains

319   homogeneous during the extrusion time. In addition, this linear evolution is linked to the

320   linear decrease of the billet length due to the constant ram velocity. As the billet length

321   linearly reduces, the surface of friction between the extruder barrel wall and the material billet

322　linearly decreases. This allows us to write the following relationship which provides us the

323　friction stress denoted K_w from a simple force balance equation:

324　$$K_w = \frac{1}{\pi.D} \frac{dF}{dL_B}$$　(5)

325　Where F is the extrusion force and L_B is the remaining billet length as defined in figure 1.

326　The third part of the curve begins when the evolution of the force versus the billet length

327　variation becomes non linear. This happens when the ram is near the die land area and

328　squeezes the static zone. The recorded force can reach a constant value or can increase with

329　the billet length decreasing. Then, the extrusion test is stopped when the billet length is equal

330　to 5 mm.

331　The analysis of the extrusion force curve allows us to restrain the data analysis to the second

332　part of the curve (linear decrease of the force) which provides us a friction stress value. The

333　use of the developed extruder provides the evolution of both the friction force along the

334　extruder barrel wall and the total extrusion force as shown in figure 5. The slopes of the

335　friction force curve and total force curve are very close (deviation of 3%). This indicates that

336　the two measurements provide the same information as both curves allow for the computation

337　of the friction stress K_w using eq. (5). Testing visco-plastic non compressible material helps us

338　to show the efficiency of the two data analysis procedures. The effects of both shaping and

339　friction force along the extruder barrel on the total extrusion force is highlighted. Finally, with

340　the illustration given in figure 5, the computation of the friction stress K_w with eq. 5 can be

341　performed with the data obtained from both the total extrusion force and the measured friction

342　force data.

343　The difference between the total extrusion force F and the friction stress F_{fr} provides a quasi-

344　constant value which is not influenced by the ram advance as shown in figure 5. This force is

345　considered to be equal to the shaping force F_{pl} required to reduce the billet diameter from D to

346　d. The resulting force value, denoted F_{pl} can be used to compute an elongational or a shear

14

347 yield stress and a velocity factor which can be linked to the consistency and the flow index of

348 the tested material (Avitzur 1983; Basterfield et al. 2005; Benbow and Bridgwater 1993;

349 Horrobin 1999; Kobayashi and Thomsen 1963; Mimoune and Aouadja 2004; Toplak et al.

350 2007; Hill 1950). In addition, F_{pl} can be computed from the total extrusion force curve when

351 the remaining billet length is equal to the dead zone length L_{dz} estimated with eq. (4). Eq. (4)

352 provides L_{dz} value equal to 13.65 mm. At this value of billet length, the total extrusion force is

353 equal to 716 N. This force is close to the difference between the measured total extrusion

354 force and the measured friction force (F_{pl} = 693 N – standard deviation of 3.3%).

355 This measured value of F_{pl} is later used to study the rheological behaviour of the studied

356 viscoplastic paste.

357

358 **3.2. Friction force data analysis**

359 The aim of the data analysis is to obtain the relationship between the ram velocity and the

360 friction stress acting along the extruder barrel wall as proposed by eq. (3).

361 The friction stress value is obtained from the linear part of the evolution of the total force (or

362 the friction force) versus the remaining billet length L_B as proposed in the previous section

363 and as shown in figure 6 for soft modelling clay. As expected, the slope of the curve does not

364 depend on the extrusion ratio d/D but is influenced by the ram velocity. From figure 6, it is

365 observed that the computed slope values for different d/D and same ram velocity are very

366 close.

367 In figure 7, computed friction stress K_w is plotted versus the ram velocity for the three tested

368 materials. The best fit of the friction law is given for each of them. We note that the friction

369 law given by eq. (3) is able to describe the friction behaviour of all tested materials as the R^2

370 coefficient is always higher than 0.99. In order to ensure the accuracy of the proposed method

371 (geometry non-dependency) two extruder barrel diameters were tested. Both diameters

372 provide the same K_w values. This confirms the consistency of the proposed method as it does

373 not depend on the extruder geometry, but seems to provide only material friction parameters.

374 It should be noted that the extruder wall roughness is the same in both cases (same steel and

375 same machining to obtain an average roughness of 3 μm). Such parameters could have large

376 effects on the measured friction stress, but this is out of scope of the present work (Hoang et

377 al. 2010).

378 For soft modelling clay, the obtained friction yield stress value is 31 ± 2 kPa. This value is

379 close to those obtained with rotating smooth cylinder and back extrusion technique given in

380 section 2.1 (deviation of respectively 3 and 15%). For kaolin, extrusion tests provide a friction

381 yield stress of 8.7 ± 1 kPa. This is close the values obtained with the back extrusion technique

382 and smooth cylinder given in section 2.1 (maximum deviation of 9%).

383

384   **3.3. Shaping force analysis**

385 The required pressure drop to ensure the flow of a visco-plastic fluid through an extruder die

386 is commonly modelled by two contributions: The friction forces acting on the material/die

387 interface and the force required for the internal bulk deformation (Benbow and Bridgwater

388 1993; Benbow et al. 1991).

389 In our case, the recorded shaping force F_{pl} required to ensure the flow in the tapered die land

390 (as we considered that the dead zone acts as a conical convergent die) is precisely the sum of

391 three contributions:

392   -   The force required for bulk deformation $F_{pl,1}$. It corresponds to the plastic work needed

393   to reduce the billet diameter.

394   -   The force required to overcome the friction on the dead zone which is considered here

395   as a tapered die $F_{pl,2}$.

396   -   The force required to overcome the friction on the exit orifice surface $F_{pl,3}$.

397 The analysis of the force required for the plastic work to reduce the diameter of the material

398 billet ($F_{pl,1}$) has been the subject of numerous studies. The most used data analysis is given by

399 Benbow and Bridgwater (Benbow and Bridgwater 1993) and have been used successfully to

400 describe the flow of many materials (Alfani and Guerrini 2005; Basterfield et al. 2005; Li and

401 Bridgwater 2000; Mascia et al. 2006; Rabideau et al. 2010; Zhou and Li 2005a; Zhou and Li

402 2005b). This equation writes:

403
$$F_{pl,1} = \frac{\pi D^2}{2}.\left(\sigma_0 + \alpha V^{n_{BB}}\right)\ln\left(\frac{D}{d}\right) \tag{6}$$

404 Where σ_0 is considered as the elongational yield stress, α and n_{BB} are fitting parameters which

405 depend on the material rheological behaviour. As proposed by Adams et al. (Adams et al.

406 1997), for a material respecting the Von Mises criterion, the plastic elongational yield stress is

407 equal to $3^{1/2}\tau_0$. The main limitation of this model is that α and n_{BB} are not material intrinsic

408 parameters.

409 Basterfield et al. attempt to improve the modelling of the velocity influence on the extrusion

410 force. This model is adapted from the Gibson equation to be able to describe viscoplastic

411 fluids (Basterfield et al. 2005). Assuming a spherically convergent flow (with a dead zone

412 angle of 45°) and neglecting the contribution due to shear, the author proposed an alternative

413 modelling. They considered the modelling of the flow in a conical duct with an angle around

414 45° where the shear contribution can be neglected. Finally, the author derived the equation

415 (the transitions between conical and cylindrical flows at both the dead zone and the exit

416 orifice entrance are neglected):

417
$$F_{pl,1} = \frac{\pi D^2}{4}.\left[2\sqrt{3}\tau_0 \ln\left(\frac{D}{d}\right) + \frac{2k_s\sqrt{3}^{n_s+1}}{3n_s.2^{n_s}}\left(\frac{2V.D^2}{d^3}\right)^{n_s}\sin\theta(1+\cos\theta)^{n_s}(1-(d/D)^{3n_s})\right] \tag{7}$$

418 With n_s and k_s represent respectively the flow index and the flow consistency. We note that

419 when the ram velocity tends to 0, eq. (7) reduces to eq. (6). Equation (7) is finally used in the

420 present study to evaluate the force contribution linked with internal deformation.

421 Then, the force required to overcome the friction on the tapered dead zone surface is

422 computed using the modelling given by Benbow and co-authors (Benbow and Bridgwater

423 1993; Benbow et al. 1991). It is important to note that the friction stress acting on the dead

424 zone surface differ from the friction stress acting on the steel barrel (the interface roughness is

425 different). Moreover, in this particular case, the tribological behaviour implies a

426 material/material interface. As a consequence, it seems rational to consider the friction at such

427 interface as a thin localized shear band. Thus, as used for squeeze geometry (Sherwood and

428 Durban 1996, 1998; Engmann et al. 2005), it is assumed that the friction stress at the extruder

429 barrel is a fraction of the friction stress at the dead zone interface. We define a coefficient m

430 as the ratio of the friction stress at the extruder barrel to the friction stress at the dead zone

431 interface. Moreover this coefficient m tends to K_{w0}/τ_0 when the interfacial velocity tends to 0.

432 The coefficient m can be expressed as follow:

433 $$m = \frac{K_w(\text{steel surface})}{K_w(\text{dead zone surface})} = \frac{K_{w0}}{\tau_0} \tag{8}$$

434 This coefficient allows us to write the friction force acting on the tapered dead zone surface.

435 The final expression is given by the Benbow and co-authors modelling combined with eqs.

436 (3) and (8) (Benbow and Bridgwater 1993; Benbow et al. 1991):

437 $$F_{Pl,2} = \frac{1}{m}\frac{\pi D^2}{4}\left[K_{w0}\cot\theta \ln\frac{d}{D} + k_{fr}V^{n_{fr}}\frac{D^{2n_{fr}}}{d^{2n_{fr}}}\left(1 - \left(\frac{d}{D}\right)^{2n_{fr}}\right)\right] \tag{9}$$

438 It can be noted that this assumes that the slip layer behaviour is the same against the extruder

439 barrel and against the static zone. However, it can be considered that the power law index

440 taken for the material/material interface can be equal to n_s as it concerns a material/material

441 interface. At least, the power law index ranges between n_{fr} and n_s. This could have some

442 noticeable impact that would be discussed at the end of the section.

443   The third contribution which corresponds to the friction along the die orifice steel surface (R_t

444   = 3µm) is commonly written using a simple force balance equation:

445    $$F_{Pl,3} = \pi dL_O \left[K_{w0} + k_{fr} V^{n_{fr}} \frac{D^{2n_{fr}}}{d^{2n_{fr}}} \right]$$ (10)

446   Finally, the shaping force F_{pl} is provided by the summation of the three contributions:

447    $$F_{Pl} = F_{Pl,1} + F_{Pl,2} + F_{Pl,3}$$ (11)

448   For the three tested materials, it is then possible to highlight the rheological parameters (i.e.

449   τ_0, k_s and n_s) which provide the best fit between experiments and modelling. Results are

450   shown on figures 8 to 10. Those curves show that the proposed modelling is able to provide

451   an estimation of the rheological parameters without extruder geometry dependency. This

452   conclusion is clearly presented on figure 11 where the modelled values of the shaping force

453   F_{pl} are plotted versus the measured ones. The correlation between modelling and experiments

454   is very good (R^2=0.99). The Basterfield et al. analysis applied to the used die geometry and

455   local roughness is suitable for the shaping force analysis. Rheological parameters are listed in

456   the table 1. Shear thinning behaviour characterises the three tested materials. The comparison

457   of the shear yield stress obtained by vane geometry (section 2.1) and Extrusion tests shows

458   that extrusion provides close higher values for the three tested materials. The variation is

459   more significant for of kaolin paste (35%) and cement paste (21%) and is lower for soft

460   modelling clay (11%).

461   In order to study the effect of the power law index used to compute the friction against the

462   dead zone, the computation is also made using n_s instead of n_{fr} in eq. (9). In this case, the

463   obtained consistencies and flow index changes. The consistency k_s becomes 17.5 kPa.s

464   instead of 11.5 kPa.s for the cement paste, 19.0 kPa instead of 12.8 kPa for the kaolin and 5.1

465   instead of 16.8 kPa for the soft modelling clay. The flow index n_s remains at 0.1 for the

466   cement paste but becomes 0.2 instead of 0.11 for the kaolin and 0.9 instead of 0.46 for the soft

467 modelling clay. Those values provide also a good correlation R²=0.96. This shows that the

468 assumption of the friction law against the static zone is important as it largely influences the

469 determination of the consistency and flow index. It can be advised to use conical steel die

470 with the same roughness as the barrel one to validate the use of n_{fr} in eq. (9).

471

472 **4 Conclusions**

473

474 In this study, we design a new extruder to study both the rheological and tribological

475 properties of high yield stress materials. According to literature data, the extrusion force can

476 be split into two contributions: the friction force acting along the extruder barrel and the

477 shaping force in the die land. The new device is developed that makes it possible to measure

478 both contributions. The measured friction force F_{fr} is used to study the material tribology. A

479 simple force balance equation allows us computing the friction stress acting on the barrel

480 wall. For the shaping force F_{pl}, the Basterfield et al. equation is adapted to our die geometry

481 (conical dead zone which acts as a rough tapered die). The use of our experimental data bank

482 allows us to valid our protocol of data analysis for firm materials. The method is finally used

483 to compute the Herschel-Buckley modelling parameters of the three tested materials (soft

484 modelling clay, kaolin clay and cement-based paste). Shear yield stress results are in

485 agreement with those computed from vane test shear yield stress.

486

487 **References**

488
489 Adams MJ, Briscoe BJ, Corfield GM, Lawrence CJ, Papathanasiou TD (1997) A finite
490   element analysis of the squeeze flow of an elasto-plastic paste material. Journal of
491   Non-Newtonian Fluid Mechanics 71 (1):41-57
492 Alfani R, Guerrini GL (2005) Rheological test methods for characterization of extrudable
493   cement-based materials. Materials and Structures 38 (2):239-247
494 Avitzur B (1983) Handbook of metal forming processes. New York

495 Barnes EC, Wilson DI, Johns ML (2006) Velocity profiling inside a ram extruder using
496   magnetic resonance (MR) techniques. Chemical Engineering Science 61 (5):1357-
497   1367
498 Basterfield RA, Lawrence CJ, Adams MJ (2005) On the interpretation of orifice extrusion
499   data for viscoplastic materials. Chemical Engineering Science 60 (10):2599-2607
500 Benbow JJ, Bridgwater J (1993) Paste Flow and Extrusion. Oxford
501 Benbow JJ, Jazayeri SH, Bridgwater J (1991) The flow of pastes through dies of complicated
502   geometry. Powder Technology 65 (1â€"3):393-401
503 Cheyne A, Barnes J, Wilson DI (2005) Extrusion behaviour of cohesive potato starch pastes:
504   I. Rheological characterisation. Journal of Food Engineering 66 (1):1-12
505 Dealy JM (1995) On the significance of pressure relaxations in capillary or slit flow.
506   Rheologica Acta 34 (1):115-116
507 Doll G, Händle F, Spiessberger F, Händle F (2007) Piston Extruders
508 Extrusion in Ceramics. In. Engineering Materials and Processes. Springer Berlin Heidelberg,
509   pp 259-273
510 Engmann J, Servais C, Burbidge AS (2005) Squeeze flow theory and applications to
511   rheometry: A review. Journal of Non-Newtonian Fluid Mechanics 132 (1â€"3):1-27
512 Estellé P, Lanos C, Perrot A (2008) Processing the Couette viscometry data using a Bingham
513   approximation in shear rate calculation. Journal of Non-Newtonian Fluid Mechanics
514   154 (1):31-38
515 Estellé P, Lanos C, Perrot A, Servais C (2006) Slipping zone location in squeeze flow.
516   Rheologica Acta 45 (4):444-448
517 Gibson AG (1988) Converging dies In: Collyer, A.A., Clegg, D.W. (Eds.), Rheological
518   Measurements. Barking
519 Götz J, Zick K, Kreibich W (2003) Possible optimisation of pastes and the according
520   apparatus in process engineering by MRI flow experiments. Chemical Engineering
521   and Processing 42 (7):517-534
522 Hill R (1950) Mathematical theory of plasticity. Oxford
523 Hoang VH, Melinge Y, Perrot A, Rangeard D Local properties of clay based materials under
524   tribological testing. In: 6th World Congress on Particles Technology Nuremberg,
525   Germany, 2010. p 00577
526 Horrobin DJ (1999) Theorical aspects of Paste Extrusion. University of Cambridge,
527   Cambridge
528 Horrobin DJ, Nedderman RM (1998) Die entry pressure drops in paste extrusion. Chemical
529   Engineering Science 53 (18):3215-3225
530 Jay P, Magnin A, Piau JM (2002) Numerical Simulation of Viscoplastic Fluid Flows Through
531   an Axisymmetric Contraction. Journal of Fluids Engineering 124:700-705
532 Kobayashi S, Thomsen EG (1963) Upper- and lower-bound solutions to axisymmetric
533   compression
534 and extrusion problems. International Journal of Mechanical Sciences, 7:127-143
535 Li YY, Bridgwater J (2000) Prediction of extrusion pressure using an artificial neural
536   network. Powder Technology 108 (1):65-73
537 Liddel PV, Boger DV (1996) Yield stress measurements with the vane. Journal of Non-
538   Newtonian Fluid Mechanics 63 (2-3):235-261
539 Mankar RB, Graczyk J, Gonzalvez-Alvarez A, Buggisch H Capillary rheometry studies on
540   wall slip flow of pastes. In: XIVth International Congress on Rheology, Seoul, Korea,
541   August 22-27, 2004 2004. pp RE 43-41
542 Martin PJ, Wilson DI, Bonnett PE (2006) Paste extrusion through non-axisymmetric
543   geometries: Insights gained by application of a liquid phase drainage criterion. Powder
544   Technology 168 (2):64-73

Mascia S, Patel MJ, Rough SL, Martin PJ, Wilson DI (2006) Liquid phase migration in the extrusion and squeezing of microcrystalline cellulose pastes. European Journal of Pharmaceutical Sciences 29 (1):22-34

Mimoune M, Aouadja FZ (2004) Rheometrical exploitation of experimental results obtained from new simulation device of extrusion on clay paste. Materials and Structures 37 (3):193-201

Mitsoulis E, Delgadillo-Velazquez O, Hatzikiriakos SG (2007) Transient capillary rheometry: Compressibility effects. Journal of Non-Newtonian Fluid Mechanics 145 (2):102-108

Mitsoulis E, Hatzikiriakos SG (2009) Steady flow simulations of compressible PTFE paste extrusion under severe wall slip. Journal of Non-Newtonian Fluid Mechanics 157 (1):26-33

Park H, Lim S, Laun H, Dealy J (2008) Measurement of pressure coefficient of melt viscosity: drag flow versus capillary flow. Rheologica Acta 47 (9):1023-1038

Perrot A, Lanos C, Estellé P, Melinge Y (2006) Ram extrusion force for a frictional plastic material: model prediction and application to cement paste. Rheologica Acta 45 (4):457-467

Perrot A, Lanos C, Melinge Y, Estellé P (2007) Mortar physical properties evolution in extrusion flow. Rheologica Acta 46 (8):1065-1073

Perrot A, Melinge Y, Rangeard D, Estellé P, Lanos C (2011) The back extrusion test as a technique for determining the rheological and tribological behaviour of yield stress fluids. Applied Rheology 21 (5):53642

Perrot A, Rangeard D, Melinge Y, Estellé P, Lanos C (2009) Extrusion criterion for firm cement-based materials. Applied Rheology 19 (5):53042

Rabideau BD, Moucheront P, Bertrand F, Rodts S, Roussel N, Lanos C, Coussot P (2010) The extrusion of a model yield stress fluid imaged by MRI velocimetry. Journal of Non-Newtonian Fluid Mechanics 165 (7-8):394-408

Rahman L, Rowe P, Cheyne A, Wilson DI (2002) Ram Extrusion of Potato Starch Dough Through Multi-Holed Dies. Food and Bioproducts Processing 80 (1):12-19

Roussel N, Lanos C (2003) Plastic Fluid Flow Parameters Identification Using a Simple Squeezing Test
 Applied Rheology 13:132

Sherwood JD, Durban D (1996) Squeeze flow of a power-law viscoplastic solid. Journal of Non-Newtonian Fluid Mechanics 62 (1):35-54

Sherwood JD, Durban D (1998) Squeeze-flow of a Herschel-Bulkley fluid. Journal of Non-Newtonian Fluid Mechanics 77 (1):115-121

Srinivasan R, DeFord D, Shah SP (1999) The use iof extrusion rheometry in the development of extruded fiber-reinforced cement composites. Concrete Science and engineering 1 (1):26-36

Toplak T, Tabuteau H, de Bruyn JR, Coussot P (2007) Gravity draining of a yield-stress fluid through an orifice. Chemical Engineering Science 62 (23):6908-6913

Toutou Z, Roussel N, Lanos C (2005) The squeeze test: A tool to identify firm cement-based material's rheological behaviour and evaluate their extrusion ability. Cement and Concrete Research 35 (10):1891-1899

Wildman RD, Blackburn S, Benton DM, McNeil PA, Parker DJ (1999) Investigation of paste flow using positron emission particle tracking. Powder Technology 103 (3):220-229

Yu AB, Bridgwater J, Burbidge AS, Saracevic Z (1999) Liquid maldistribution in particulate paste extrusion. Powder Technology 103 (2):103-109

Zhou X, Li Z (2005a) Characterization of rheology of fresh fiber reinforced cementitious composites through ram extrusion. Materials and Structures 38 (1):17-24

594 Zhou XM, Li ZJ (2005b) Characterization rheology of fresh short fiber reinforced
595   cementitious composite through capillary extrusion. Journal of Materials in Civil
596   Engineering 17 (1):28-35
597 Zienkiewicz OC, Jain PC, Onate E (1977) Flow of solids during forming and extrusion: Some
598   aspects of numerical solutions. International Journal of Solids and Structures 14:15-38

599

600

601 **Table Caption**

602

603 Table 1: Rheological and tribological modelling parameters obtained with vane tests and

604 extrusion for the three tested materials.

605

606 **Figure Captions**

607

608 Figure 1: Force distribution in the extrusion flow of high yield stress fluid

609 Figure 2: Dead zone length observation with soft modelling clay test extrusion (Ram velocity

610 1 mm.s^{-1}, d=16 mm and D=43.3 mm). Comparison with modelled conical dead zones.

611 Figure 3: Friction force measurement system in the designed die.

612 Figure 4: Typical evolution of the total extrusion force versus the remaining billet length.

613 Test performed on soft modelling clay, D=55.3 mm; d/D=0.36; V = 1 mm.s^{-1}.

614 Figure 5: Evolution of the friction and total extrusion force versus the remaining billet length

615 measured with the developed extruder. Test performed on Soft modelling clay: D=43.3 mm,

616 d/D=0.36, V=1 mm.s^{-1}.

617 Figure 6: Total extrusion force versus remaining billet length of soft modelling clay. Tests

618 performed for D = 43.3 mm. Slopes of linear fitting $\Delta F/\Delta L_B$ are: 4.12 (R²=0.99) for d = 8 mm

619 and V = 0.1 mm.s^{-1}; 5.21 (R²=0.96) for d = 8 mm and V = 1 mm.s^{-1}; 3.85 (R²=0.99) for d = 20

620 mm and V = 0.1 mm.s^{-1}; 5.06 (R²=0.97) for d = 20 mm and V = 1 mm.s^{-1} ;

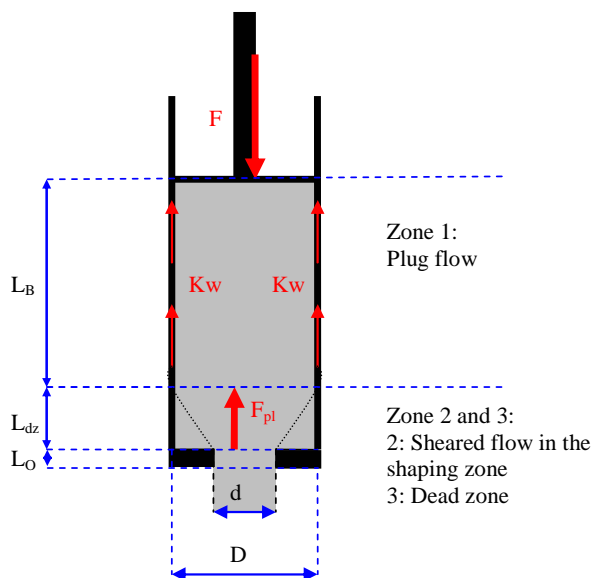621 Figure 7: Friction law obtained for the three tested materials.

622   Figure 8: Modelled and experimental values of shaping force F_{pl} for soft modelling clay

623   versus the ram advance. $\tau_0 = 56.8$ kPa ; $k_s = 16.7$ kPa.s^{ns} ; $n_s = 0.46$ are the values providing

624   the best fit for the modelling. Tests performed with D = 44.3 mm and D=55.3 mm.

625   Figure 9: Modelled and experimental values of shaping force F_{pl} for kaolin paste versus the

626   ram advance. $\tau_0 = 39.1$ kPa ; $k_s = 12.8$ kPa.s^{ns} ; $n_s = 0.11$ are the values providing the best fit

627   for the modelling. Tests performed with D = 44.3 mm and D=55.3 mm.

628   Figure 10: Modelled and experimental values of shaping force F_{pl} for cement paste versus the

629   ram advance. $\tau_0 = 19.0$ kPa ; $k_s = 11.5$ kPa.s^{ns} ; $n_s = 0.1$ are the values providing the best fit for

630   the modelling. Tests performed with D = 44.3 mm and D=55.3 mm.

631   Figure 11: Correlation between the modelled shaping force value F_{pl} and the experimental

632   value for the three tested materials.

633

634
635
636   Figure 1
637

638

Dead zone
modelled form
$L_{dz}=(D-d)/2$
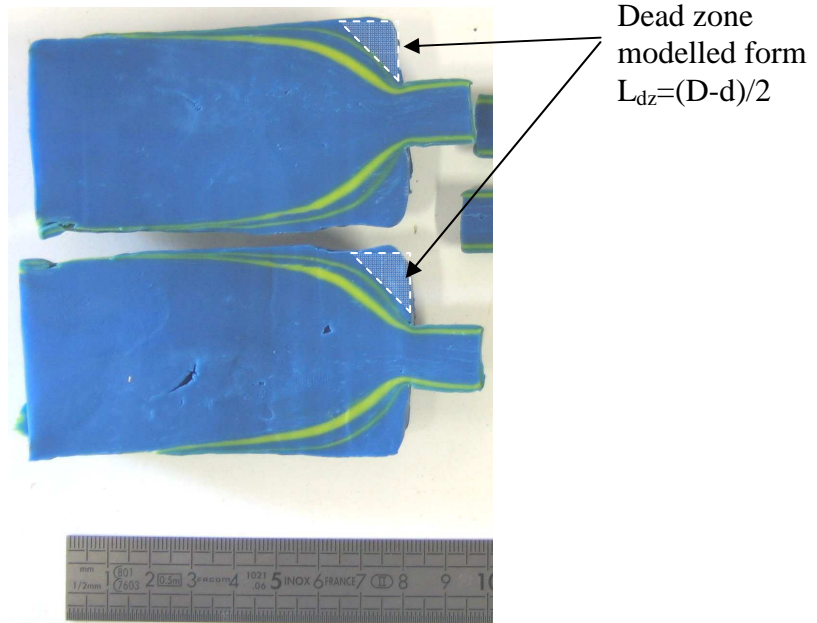
639

640

641 FIGURE 2

642
643

Extruder barrel

Pipe shoulder

Screw/bolt
system

Load cell

120°

A   A

Load cell

Die shoulder

Top view

Friction stress

20 mm
free zone

Seal ring

Dead zone

Die system

A-A

Extruder barrel
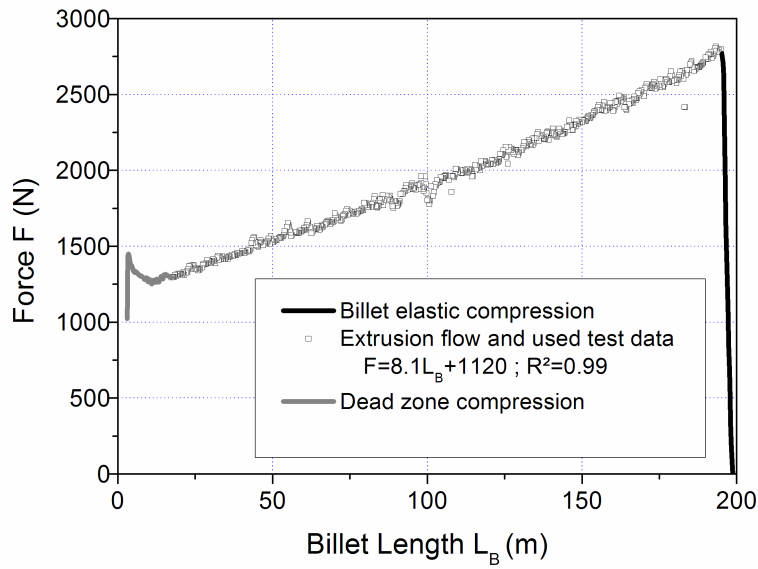
3 Load cells

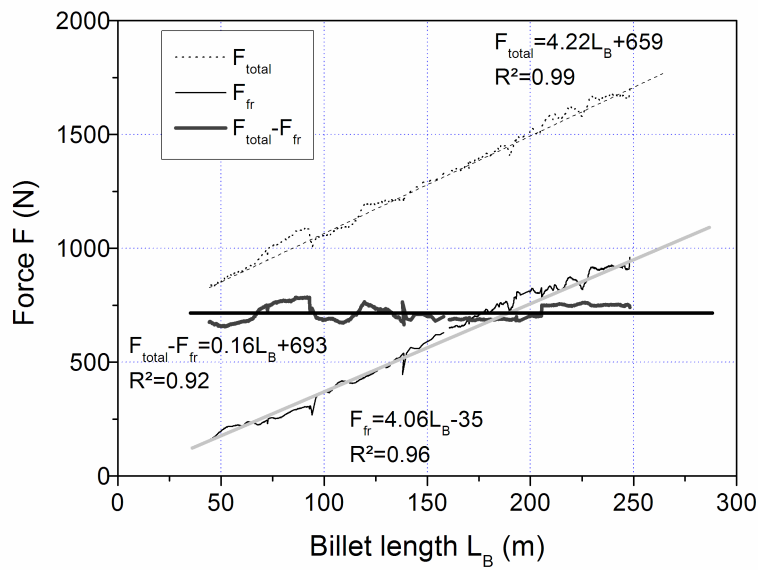Die system
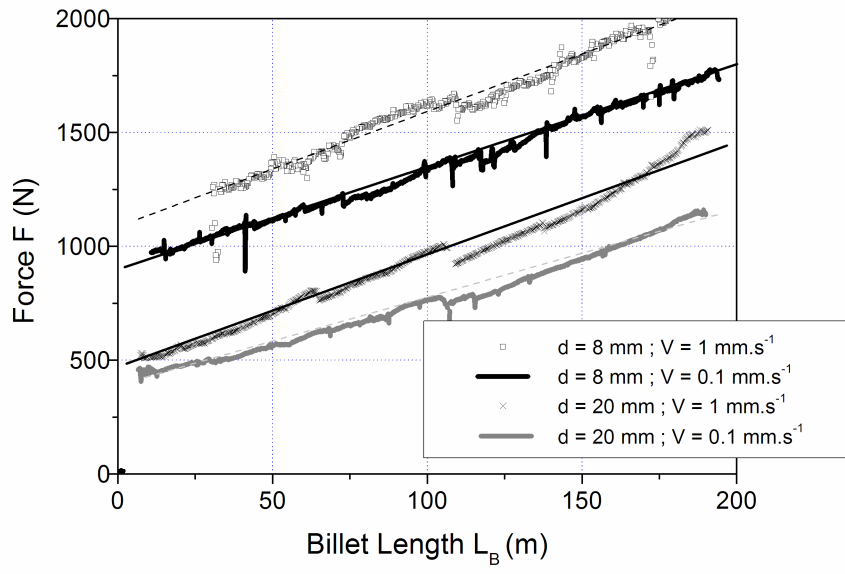
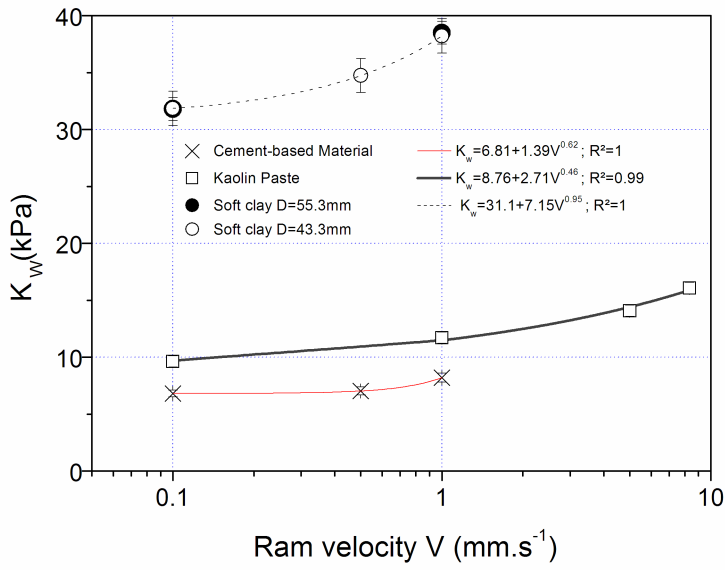3D view of separated parts
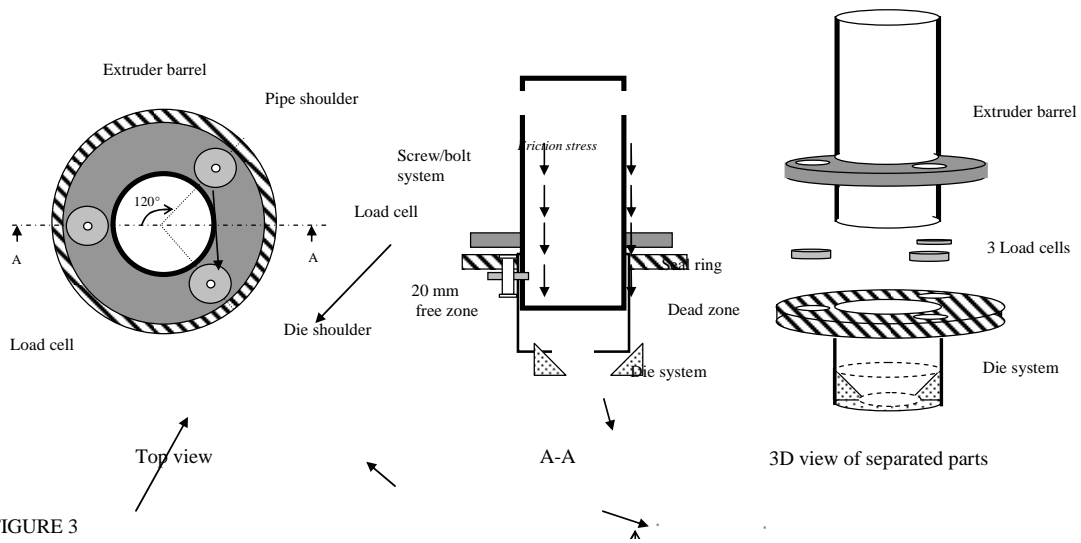
644   FIGURE 3

645

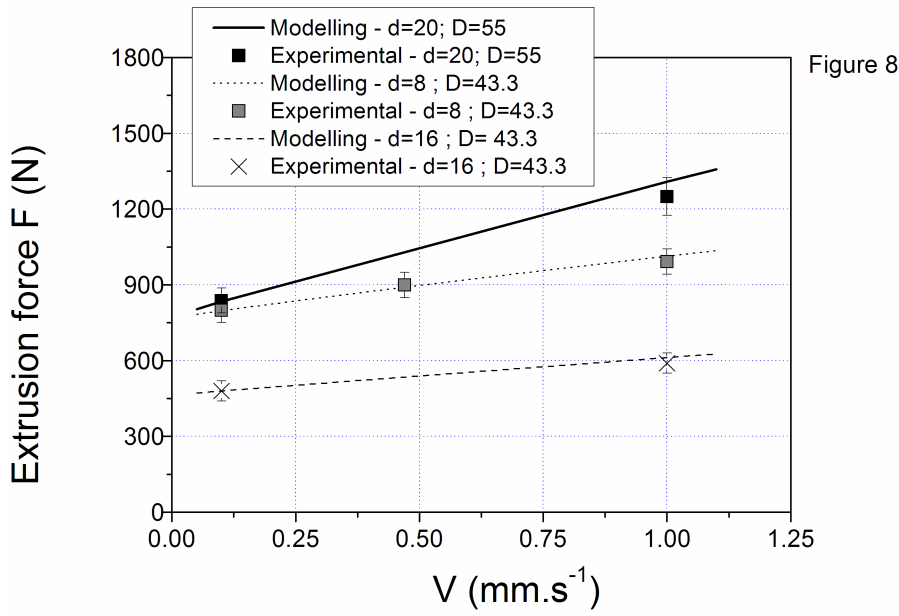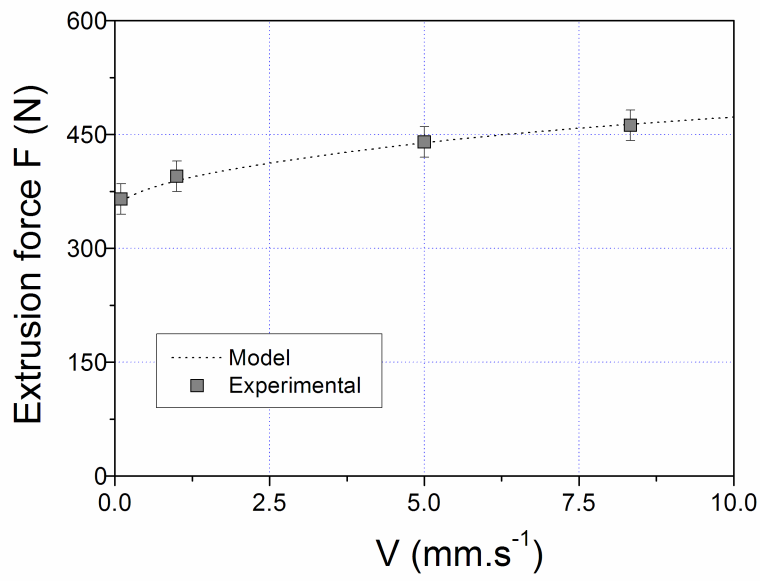Figure 4

Figure 4
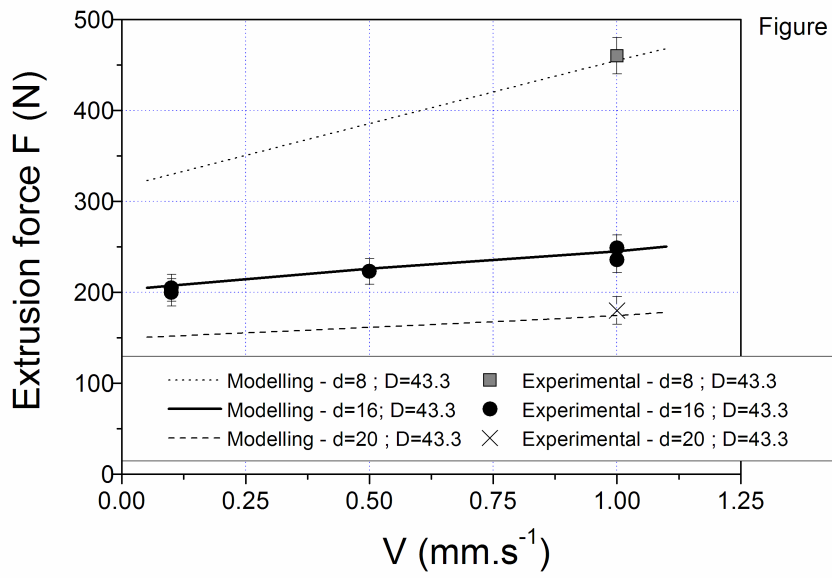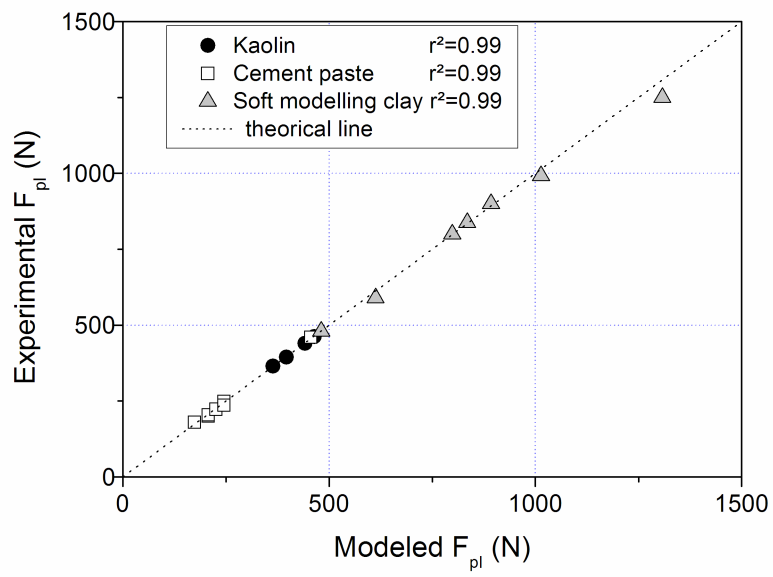
646

647

Figure 5

648

Figure 6

649

Figure 7

Figure 8

Figure 9

652

Figure 10

653

Figure 11

654